

Gravitational-Wave Lensing Fringes by Compact Dark Matter at LIGO

Sunghoon Jung^{1,*} and Chang Sub Shin^{2,†}

¹Center for Theoretical Physics, Dept. of Physics and Astronomy, Seoul National University, Seoul 08826, Korea

²Center for Theoretical Physics of the Universe, IBS, Daejeon 34051, Korea

Utilizing gravitational-wave (GW) lensing opens a new way to understand the history and structure of the universe. In spite of coarse angular resolution and short duration of observation, we show that LIGO can detect the GW lensing induced by small structures, in particular by compact dark matter (DM) of $10 - 10^5 M_\odot$, which remains an interesting DM candidate. The lensing is detected through GW frequency chirping, creating the natural and rapid change of lensing patterns: *frequency-dependent amplification and modulation* of waveforms. As a highest-frequency GW detector, LIGO is a unique GW lab to probe such light compact DM. With design sensitivity of Advanced LIGO, one-year observation can detect as many as 1000 lensed GWs and constrain compact DM fraction as small as $f_{\text{DM}} \gtrsim 10^{-3}$.

Introduction. The GW from far-away binary mergers [1, 2] is a new way to see the universe with gravitational interaction. Not only is it already revealing astrophysics of sources such as solar-mass black holes and neutron stars, but the GW can also carry information of the intervening masses and the evolution of the universe through gravitational lensing. Having the long wavelength λ , the GW is expected to be lensed by heaviest structures (such as galaxies and their clusters) with the large enough Schwarzschild radius, $2GM/c^2 = 2M \gg \lambda \simeq 2 \times 10^3 (100 \text{ Hz}/f) M_\odot$. Their prototypical lensing signal is strongly time-delayed GW images [3, 4] or statistical correlations [5].

In this letter, we show that LIGO can detect the GW lensing induced by much lighter compact structures. The new lensing observable depends crucially on the GW frequency evolution during binary inspiral and merger – “chirping”. The chirping provides the natural and rapid change of lensing patterns so that LIGO can detect relatively weak GW lensings, in spite of its coarse angular resolution (at best $\mathcal{O}(1)$ deg [6, 7], let alone typical strong-lensing image separation of arcsec or smaller) and short measurement time (less than seconds or minutes, let alone typical micro-lensing observation of a few weeks or longer). Remarkably, measuring highest GW frequencies of $f = 10 - 5000$ Hz, LIGO is a unique GW detector to see compact structures as light as $M = 10 - 10^5 M_\odot$.

An important example of such light structure is the compact DM. It remains an attractive DM candidate, predicted by various models of particle physics and cosmology: axion miniclusters, compact mini halos, and primordial black holes [8–19]. Compact DM is mainly (and most reliably) searched by light lensing: micro-lensing (temporal variation of background star brightness) [20, 21] and strong-lensing (multiple images) [22, 23]. But, in a wide range of compact DM mass $10^{-16} - 10^5 M_\odot$, its energy fraction $f_{\text{DM}} \lesssim 0.1 - 1$ remains to be probed [24]. We present the prospect for LIGO lensing observations to probe the compact DM of $M_{\text{DM}} = 10 - 10^5 M_\odot$, with the new observable.

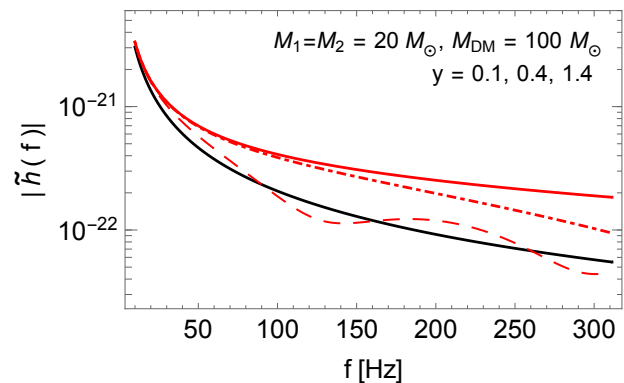


FIG. 1. Illustration of GW lensing observables at aLIGO: Lensed (red) vs. unlensed (black) waveforms in the frequency domain. The lensing compact DM mass $M_{\text{DM}} = 100 M_\odot$ and redshifted GW binary masses $M_1 = M_2 = 20 M_\odot$ merging at $f \simeq 320$ Hz. At the small impact angle $y = \theta_s/\theta_E$ (red-solid) Eq. (1), *frequency-dependent amplification* cannot be fit by a constant rescaling A_0 (Eq. (6)) of unlensed waveforms (black); whereas, at large y (dashed), *frequency-dependent modulation* cannot be matched by a constant phase-shift ϕ_0 (Eq. (5)). In general (dotdashed), both lensing effects co-exist.

GW Lensing Observable. The proposed GW lensing observable relies on the unique properties of the GW lensing (in contrast to the light lensing). Although the GW and light follow the same null-geodesic in a vacuum, they feel intervening gravitational potential differently in a few remarkable ways.

Above all, the binary GW frequency chirps. It provides the natural change of lensing patterns that is extremely useful in lensing detection. Suppose that some strong lensing creates two GW images with (small) time-delay Δt_d . The two images interfere since LIGO cannot resolve them. Then, the phase-shift between them $\sim f \Delta t_d$ grows with the frequency, and the resulting interference pattern *changes* with chirping [25, 26] (see Fig. 1 dashed) – frequency-dependent modulation. The final stage of binary inspiral (observed by LIGO) is where the frequency-dependent signal can be detected most efficiently because

the frequency is highest and grows most rapidly.

Secondly, the GW wavelength is much longer than that of light. Depending on the wavelength, lensing does not always produce two images with constant time-delay. In general, the lensed GW waveform, $\tilde{h}^L(f)$, is a superposition of all unlensed waveforms, $\tilde{h}(f)$, that follow all possible null rays (passing $\vec{\theta}$ in the thin lens plane at redshift z_L) [27, 28]

$$\tilde{h}(f)^L = \frac{d_L d_S (1+z_L)}{i d_{LS}} f \int d^2 \vec{\theta} \exp [i 2 \pi f \Delta t_d(\vec{\theta}, \vec{\theta}_s)] \tilde{h}(f), \quad (1)$$

with $d_{L,S,LS}$ the angular-diameter distance to the lens, source and between them; the source impact angle $y = \theta_s / \theta_E$ normalized by the Einstein angle $\theta_E = \sqrt{\frac{4GM_L}{c^2} \frac{d_{LS}}{d_L d_S}}$ is used, and the compact DM is treated as a point lens. Only when the GW frequency is larger than the typical time-delay between null rays $f \Delta t_d \simeq 4f M_{DM} \simeq 2 \times 10^{-5} (M_{DM}/M_\odot) (f/\text{Hz}) \gg 1$ (equivalently, $\lambda \ll M_{DM}$), the integral is dominated by discrete stationary points with separate images (geometric optics limit). In the opposite limit, GW diffraction becomes important and lensing becomes weaker (wave optics limit); eventually, the GW does not see the lens if its wavelength becomes too long.

In particular, the GW wavelength in the LIGO band, $\lambda \simeq 2 \times 10^3 (100 \text{ Hz}/f) M_\odot$, is comparable to the Schwarzschild radius $2M_{DM}$ of the compact DM of $M_{DM} = 10 - 10^5 M_\odot$. Chirping from 10 Hz to $\mathcal{O}(100 - 1000)$ Hz, GW lensing by such masses may transition from wave-optics (where $\lambda_{GW} \gtrsim 2M_{DM}$ so that lensing is weak or absent) to geometric-optics regimes (where $\lambda_{GW} \lesssim 2M_{DM}$ maximizing lensing). Therefore, with chirping, GW lensing magnitude (both amplification and time-delay) also grows; compare low and high frequency regions in Fig. 1.

The two effects combined – *frequency-dependent amplification and modulation* – define our “GW fringe” lensing signal. Fig. 1 illustrates how the fringe is detectable based on the comparison with unlensed standard waveforms. Below, we will calculate the detection efficiency of the fringe at LIGO, lensing optical depth, detection rate, and finally constraint on the compact DM fraction.

Analysis for Lensing Detection. In the LIGO frequency band, GWs from binary mergers (with redshifted $M_1 = M_2$ in this work) spend only a few seconds or minutes. Therefore, a detector is almost at rest (in spite of Earth rotation) during a whole measurement period. Then, the unlensed GW waveform is sinusoidal when observed by a single LIGO detector

$$h(t) = A_+(t) F_+ \cos \phi(t) + A_\times(t) F_\times \sin \phi(t) \quad (2)$$

$$= A(t) \cos(\phi(t) + \phi_0),$$

with detector response functions $F_{+,\times}$ constant in time during the measurement period. Rather, the time depen-

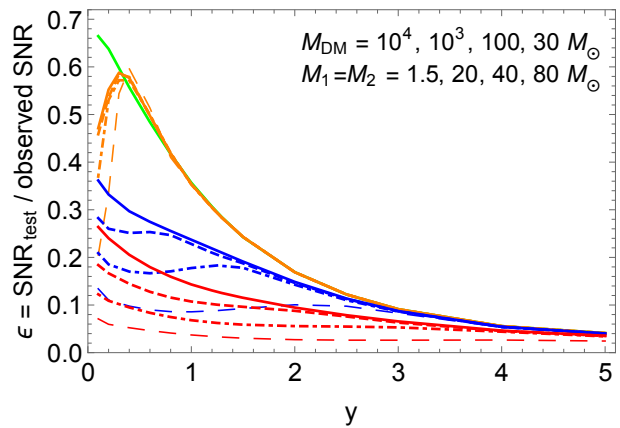


FIG. 2. The lensing-detection efficiency ϵ in Eq. (10) of a single aLIGO detector with design sensitivity. Lensing DM masses are $M_{DM} = 10^4, 10^3, 100, 30 M_\odot$ and redshifted GW binary masses $M_1 = M_2 = 1.5$ (solid), 20 (dashed), 40 (dot-dashed), 80 (long-dashed) M_\odot .

dences of amplitude and phase are determined uniquely by the redshifted chirp mass $\mathcal{M}_z = (M_1^3 M_2^3 / (M_1 + M_2))^{1/5}$ at the leading Newtonian order

$$A(t) \propto \mathcal{M}_z^{5/3} f(t)^{2/3}, \quad (3)$$

$$\frac{df(t)}{dt} = \frac{96}{5} \pi^{8/3} f^{11/3} \mathcal{M}_z^{5/3}. \quad (4)$$

Now, the unlensed waveform observed in the frequency domain is simply

$$\tilde{h}(f) = \tilde{A}(f) \exp[i(\Psi(f) + \phi_0)], \quad (5)$$

where

$$\tilde{A}(f) = A_0 \mathcal{M}_z^{5/6} f^{-7/6}, \quad (6)$$

$$\Psi(f) = 2\pi f t_c + \frac{3}{128} (\pi \mathcal{M}_z f)^{-5/3}, \quad (7)$$

and any constant phase-shift is absorbed into ϕ_0 . Although the real-valued constant A_0 depends on various source parameters (such as polarization and distance), single short measurement can only measure A_0 .

We ignore spin-induced effects, binary-orbit eccentricity and post-Newtonian corrections. All LIGO events so far have small spins consistent with zero. The eccentricity near merger is small since a binary orbit quickly circularizes. However, as they may cause frequency-dependent modulations (mimicking GW fringes), it is worthwhile including them in future studies.

We use the χ^2 least-squares fit method to determine whether GW lensing can be detected. We define the significance of the fit between lensed (observed) and unlensed (trial template) waveforms as

$$(\text{SNR}_{\text{test}})^2 \equiv 4 \int_{f_0}^{f_1} \frac{|\tilde{h}(f)^L - \tilde{h}(f)_{\text{best-fit}}|^2}{S_n(f)} df, \quad (8)$$

similarly to the observed signal-to-noise ratio (SNR)

$$(\text{SNR})^2 = 4 \int_{f_0}^{f_1} \frac{|\tilde{h}(f)|^2 L^2}{S_n(f)} df. \quad (9)$$

The integration is done over a whole measurement period of the aLIGO frequency band [29]: $f_0 = 10$ Hz, $f_1 = \min(f_{\text{ISCO}}, 5000 \text{ Hz})$, where we integrate up to the innermost stable circular orbit (ISCO) at $r = 3(M_1 + M_2)$ with $f = f_{\text{ISCO}} = (3\sqrt{3}\pi(M_1 + M_2))^{-1}$ Hz.

For the given observed lensed-waveform $\tilde{h}(f)^L$, we find the best-fit unlensed waveform $\tilde{h}(f)_{\text{best-fit}}$ by minimizing SNR_{test} over the two fitting parameters, A_0 and ϕ_0 . Here, we assume that the chirp mass \mathcal{M}_z and the coalescence time t_c (time at f formally diverges) are well measured regardless of lensing effects; indeed, \mathcal{M}_z is often measured exquisitely well via specific waveform evolution over many GW cycles [30]. The simplified best-fit based on A_0 and ϕ_0 is good enough to simulate fringe-detection physics, as illustrated in Fig. 1; *frequency-dependent amplification and interference modulation cannot be fit by unlensed standard waveforms*.

We regard that the existence of GW lensing is detected if $\text{SNR}_{\text{test}} \geq 3$ or 5 in addition to $\text{SNR} \geq 8$ (for reliable discovery); when considering three aLIGO detectors in the final results, we require the total SNR quadrature-sum to satisfy these criteria. Although more dedicated analysis can be useful, we do not study here. It is useful to define the lensing-detection efficiency of a detector as

$$\epsilon \equiv \frac{\text{SNR}_{\text{test}}}{\text{SNR}}. \quad (10)$$

The ϵ is shown in Fig. 2 for a single aLIGO detector with design sensitivity (see below). It is typically $\sim \mathcal{O}(10)\%$ so that strong GWs with $\text{SNR} \sim \mathcal{O}(10)$ can be detected to be lensed with $\text{SNR}_{\text{test}} \sim \mathcal{O}(1)$. The heavier the lens, the larger ϵ , trivially. The lighter GW binaries, the larger ϵ ; it is because lighter GWs merge at higher frequencies experiencing more modulation.

The slight fluctuation and drop of the ϵ curve in Fig. 2 are related to the interplay of frequency-dependent modulation and amplification. The former becomes more significant at large- y due to larger time-delay, whereas the latter at small- y due to stronger lensing, as illustrated in Fig. 1. Intermediate regimes may produce less exotic waveforms (e.g., dot-dashed in Fig. 1), if the GW merges just before its frequency reaches the first destructive interference, hence slightly lower ϵ producing the fluctuations. Also, ϵ starts to drop at smaller y for heavier DM lenses (stronger time-delay) and lighter GW binaries (merging at higher frequency).

Advanced LIGO Prospects. We turn to discuss expected results from three aLIGO detectors, representing the network of two aLIGO and one VIRGO detectors, with design aLIGO sensitivity (the dark-blue curve in

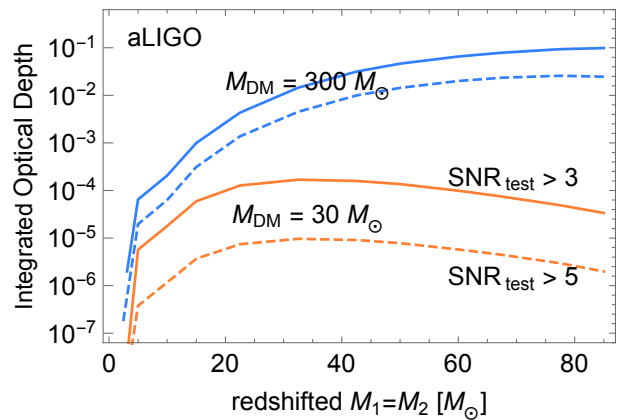


FIG. 3. The optical depth of the given GW source mass integrated over the source distance as in Eq. (12). It is the probability for detectable lensing, thus including the probability to have $\text{SNR}_{\text{test}} > 3$ (solid) or 5 (dashed) and $\text{SNR} > 8$ from three aLIGO detectors with design sensitivity. The upper (lower) set of curves is for lensing $M_{\text{DM}} = 300$ (30) M_{\odot} .

Fig.1 of Ref. [29]), yielding ~ 3 times larger SNR (thus, seeing ~ 3 times farther distance) than current LIGO. We use LIGO to represent any GW detectors working in the LIGO frequency band with similar sensitivity.

The differential optical depth of the GW source with \mathcal{M} at z_S and the gravitational lens with M_L at (z_L, y) is

$$\begin{aligned} d\tau &= d\tau(M_L, z_L, y; \mathcal{M}, z_S) \\ &= dz_L \frac{ca(z_L)}{H(z_L)} 2\pi(d_L\theta_E)^2 y dy (1+z_L)^3 n_L P(w) \quad (11) \\ &= \frac{3}{2} f_{\text{DM}} \Omega_{\text{DM}} dz_L \frac{H_0^2}{H(z_L)c} (1+z_L)^2 \frac{d_L d_{LS}}{d_S} 2y dy P(w), \end{aligned}$$

with the comoving DM density n_L (that we assume to be constant in z_L) and the probability $P(w)$ for large enough SNR (that depends on all source and lens parameters; see below). In the standard FRW cosmology with $\Omega_m = 0.27$, $\Omega_{\text{DM}} = 0.24$ and $\Omega_{\Lambda} = 0.73$ denoting the energy-density fraction of matter, DM and cosmological constant, $H(z)^2 = H_0^2(\Omega_m(1+z)^3 + \Omega_{\Lambda})$. f_{DM} is the fraction of the compact DM energy density to that of the total DM. The integrated optical depth is

$$\tau = \int_0^{z_S} dz_S \int_0^{z_S} dz_L \int_0^y dy d\tau, \quad (12)$$

where most contributions come from $z_S \lesssim 2$ and $y \lesssim 6$; see Appendix. For small τ , the lensing probability is $1 - e^{-\tau} \simeq \tau$.

The optical depth represents the probability for *detectable* lensing of the given source mass. The function $P(w)$ already includes the lensing detection efficiency ϵ and the observed SNR distribution for three aLIGO detectors ($w \leq w_{\text{max}} = 1.4$); refer to Appendix and Ref. [31] for more details. In other words, $P(w)$ is the probability

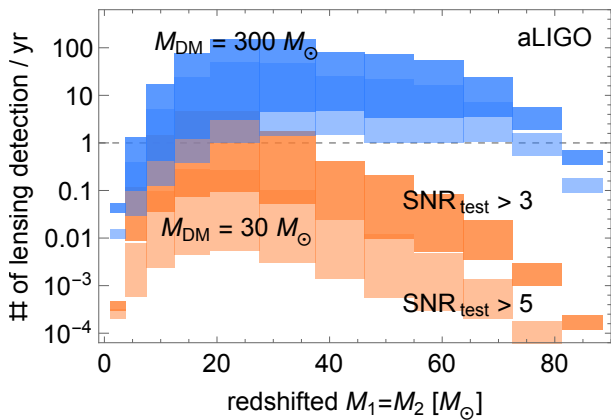


FIG. 4. The number of GW lensing detections per year by three aLIGO detectors with design sensitivity, representing the aLIGO-VIRGO network. The darker (lighter) region satisfies $\text{SNR}_{\text{test}} > 3$ (5) and $\text{SNR} > 8$ for lensing detection, and vertical ranges span between the optimistic merger-rate model M1 and the pessimistic model M3 [32]. The blue (orange) region is for the lensing DM mass $M_{\text{DM}} = 30$ (300) M_{\odot} . The horizontal dashed line denotes one detection per year.

for observed $\text{SNR} \geq 3/\epsilon$ or $5/\epsilon$, depending on the criteria $\text{SNR}_{\text{test}} \geq 3$ or 5.

Fig. 3 shows the integrated optical depth Eq. (12) for the given source mass. It is lowest for lightest binaries mainly because GWs are weakest so that the relevant comoving volume of the lens and source is smallest; in log-log scale, the curves in Fig. 3 become mostly linear. Secondly, it peaks at $\mathcal{M}_z \sim 30M_{\odot}$ for $M_{\text{DM}} = 30M_{\odot}$, as ϵ is smaller for heavier binaries (Fig. 2). But it keeps growing with the binary mass for heavy $M_{\text{DM}} = 300M_{\odot}$, since ϵ from stronger lensing depends less on the binary masses (Fig. 2). Lastly, requiring tighter criteria loses more detections for the lighter DM; it is because most lensing detections for the lighter DM are made with smaller SNR_{test} near the detection threshold.

The differential merger rate of the source with \mathcal{M}, z_S is obtained with relevant differential comoving volume

$$d\dot{N}_{\text{merger}} = dz_S d\mathcal{M}_z \frac{4\pi\chi(z_S)^2 c}{H(z_S)} \frac{d\dot{n}_{\text{merger}}}{d\mathcal{M}_z}. \quad (13)$$

For the comoving merger-rate density $\dot{n}_{\text{merger}}/d\mathcal{M}_z$, we take the two sets of values from Fig.3 of Ref. [32]: one from the merger-rate model M1, optimistically predicting the highest merger-rate consistent with LIGO's observations so far, and the other from the pessimistic model M3 predicting the lowest merger-rate. The values are the local (averaged over $z_S \leq 0.1$) merger-rate density, and we use these local values for all z_S , for simplicity. But, as the merger-rate actually grows with z_S up to $z_S \simeq 2$ [32], our estimation is conservative, and a more careful estimation is worthwhile.

Finally, we obtain the total number of GW lensing detections per year, by multiplying the differential merger

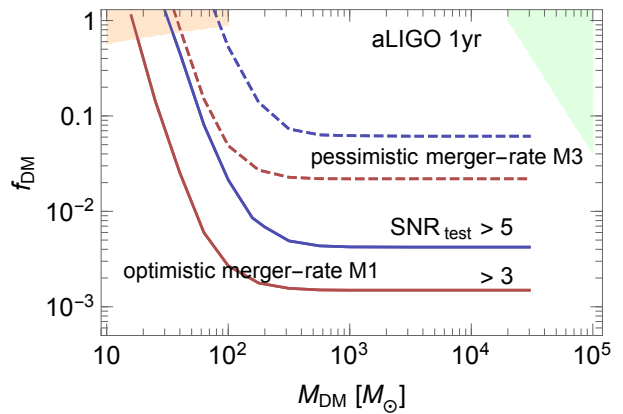


FIG. 5. Expected sensitivities on compact DM fraction f_{DM} from one-year observation by three aLIGO detectors with design sensitivity. Regions above each line is constrained. Lensing detection criteria $\text{SNR}_{\text{test}} > 3$ (red) or 5 (blue) is used with optimistic merger-rate model M1 (solid) or pessimistic model M3 (dashed). Shaded regions are constrained by light lensing measurements [21, 23].

rate Eq. (13) by the differential optical depth Eq. (11), $\dot{N}_{\text{lensing}} = \int d\tau d\dot{N}_{\text{merger}}$. The total number of detections is shown in Fig. 4, decomposed into the contribution from each GW binary mass. Optimistic yearly detections are 13 (640) for $M_{\text{DM}} = 30$ (300) M_{\odot} with $\text{SNR}_{\text{test}} > 3$ and 0.79 (200) with $\text{SNR}_{\text{test}} > 5$. Pessimistic expectations are about 20-50 times smaller. Most lensing detections are expected from $\mathcal{M}_z = 20-30M_{\odot}$ mainly because it is where most binary mergers are predicted too [32]. In addition, many behaviors discussed in Fig. 3 are similarly reflected in Fig. 4.

As many detections can be made in a year, we can also express the prospects in terms of the expected constraint on the compact DM fraction f_{DM} , by assuming no GW fringe will be detected. The expected constraints are shown in Fig. 5 for one-year observation; $1/f_{\text{DM}}$ shown simply corresponds to the expected number of detections. The constraints start from $M_{\text{DM}} \sim 10M_{\odot}$, become strongest for $M_{\text{DM}} \gtrsim 10^2 M_{\odot}$, and stop shown for $M_{\text{DM}} \gtrsim 10^5 M_{\odot}$. The three regions have different values of the phase-shift

$$f\Delta t_d \simeq 2 \times 10^{-5} (M_{\text{DM}}/M_{\odot})(f/\text{Hz}) \quad (14)$$

(in the wave-optics regime, we can think of Δt_d as a typical time-delay from null rays with $\theta \simeq \theta_E$).

For $f\Delta t_d \gtrsim 0.1$ from $M_{\text{DM}} \gtrsim 10^2 M_{\odot}$, the GW fringe is most pronounced, and LIGO fringe search is a powerful probe of those compact DM. Here, the $\mathcal{O}(1)$ evolution of the frequency in the LIGO band produces $\gtrsim \mathcal{O}(1)$ cycles of fringe patterns, which is easiest to detect. Resulting optimistic constraint $f_{\text{DM}} \lesssim 10^{-3}$ is comparable to or stronger than existing constraints from light lensing measurements [21, 23] and proposed searches [33]. The constraint will further improve, linearly with the observa-

tion time; and the final upgrade of aLIGO (the light-blue curve in Ref. [29]) will detect sources up to $z_S \simeq 3 - 4$ detecting $\sim 10 - 100$ times more events.

The strong limit is attributed to a large merger rate and large optical depth. Not only can LIGO see sources at far distance ($z_S \lesssim 2$ in this paper, but farther with future upgrades), but also at large y too. Remarkably, large $y \gtrsim 1.5$ can still lead to the sizable efficiency $\epsilon = 5 - 25\%$ in Fig. 2. Although lensing is weak, the GW amplitude amplification/modification can still be $\sim 10\%$ (4%) for $y = 3$ (5). Combined with frequency-dependent interference and diffraction over a range of frequency, this can lead to such sizable ϵ . On the contrary, light lensing is observed through its brightness so that large- y lensing effects are hardly observable.

It is also notable that constraints become almost constant for heavy masses $M_{\text{DM}} \gtrsim 500M_\odot$ in Fig. 5. It is because the decrease of the DM number density (with heavier DM) is compensated exactly by the increase of the Einstein radius in the last line of Eq. (11); the optical depth then depends on the DM mass only indirectly via detector effects encoded in $P(w)$. Nevertheless, we stop showing the result at $M_{\text{DM}} \sim 10^5 M_\odot$, since waveform modulation with $f\Delta t_d \gtrsim 10^3$ in the heavier region maybe too quick to be temporally resolved (or time-delay may be too large; see Appendix). We encourage dedicated studies, but our main results for the lighter DM will not change.

On the other hand, LIGO fringe search is not sensitive to $M_{\text{DM}} \lesssim \mathcal{O}(10)M_\odot$. Here, small phase-shift $f\Delta t_d \lesssim 0.1$ and weak lensing barely produce observable GW fringes.

In general, a lensing fringe becomes most pronounced when the following relation between the GW frequency f and the compact DM mass M_{DM} is satisfied

$$(M_{\text{DM}}/M_\odot)(f/\text{Hz}) \gtrsim 10^4 - 10^6, \quad (15)$$

equivalent to $f\Delta t_d \gtrsim 0.1 - 10$ from Eq. (14). The maximum $f\Delta t_d$ (hence, $M_{\text{DM}}f$) depends on the detector's temporal resolution, as discussed. But, it is clear that, as LIGO is a highest-frequency GW detector, $M_{\text{DM}} = 10 - 10^5 M_\odot$ can be seen by GW only at LIGO. A smaller-frequency GW detector (such as LISA) can probe only correspondingly heavier DM. In the meantime, this discussion applies also to the light fringe. Indeed, the compact DM of $10^{-16} - 10^{-14} M_\odot$ is expected to produce (femto-lensing) fringes on gamma-ray bursts (GRBs) with $f_{\text{GRB}} \simeq 10 - 1000 \text{ keV} \simeq 2.4 \times (10^{18} - 10^{20}) \text{ Hz}$ [34], satisfying Eq. (15) and (14) again. Although the GRB frequency does not change with time, the relative spectral fringe can be observed [35].

Conclusion. We have shown that LIGO can detect the GW lensing fringe induced by the compact DM of $M_{\text{DM}} = 10 - 10^5 M_\odot$. The LIGO measurement of GW fringes can surpass or strengthen existing constraints on such DM fraction, as shown in Fig. 5. Without LIGO

fringe measurements, this small structure could not have been probed with GW. Meanwhile, based on the general relation Eq. (15) of the fringe, lower-frequency GW detectors can probe heavier (DM) structures. Therefore, future broadband GW surveys covering $f = 10^{-9} - 10^3 \text{ Hz}$ (from various detectors) will accurately measure a wide range of structures through the GW lensing fringe.

Acknowledgements. We thank Hyung Mok Lee and Hyung Won Lee for useful comments. SJ is supported by Korea NRF-2017R1D1A1B03030820 and NRF-2015R1A4A1042542. CSS is supported by IBS under the project code IBS-R018-D1.

* sunghoonj@snu.ac.kr

† csshin@ibs.re.kr

- [1] B. P. Abbott *et al.* [LIGO Scientific and Virgo Collaborations], Phys. Rev. Lett. **116**, no. 6, 061102 (2016) doi:10.1103/PhysRevLett.116.061102 [arXiv:1602.03837 [gr-qc]].
- [2] B. P. Abbott *et al.* [LIGO Scientific and Virgo Collaborations], Phys. Rev. Lett. **119**, no. 16, 161101 (2017) doi:10.1103/PhysRevLett.119.161101 [arXiv:1710.05832 [gr-qc]].
- [3] M. Sereno, A. Sesana, A. Bleuler, P. Jetzer, M. Volonteri and M. C. Begelman, Phys. Rev. Lett. **105**, 251101 (2010) doi:10.1103/PhysRevLett.105.251101 [arXiv:1011.5238 [astro-ph.CO]].
- [4] A. Pirkowska, M. Biesiada and Z. H. Zhu, JCAP **1310**, 022 (2013) doi:10.1088/1475-7516/2013/10/022 [arXiv:1309.5731 [astro-ph.CO]].
- [5] P. Laguna, S. L. Larson, D. Spergel and N. Yunes, Astrophys. J. **715**, L12 (2010) doi:10.1088/2041-8205/715/1/L12 [arXiv:0905.1908 [gr-qc]].
- [6] B. P. Abbott *et al.* [LIGO Scientific and VIRGO Collaborations], Living Rev. Rel. **19**, 1 (2016) doi:10.1007/lrr-2016-1 [arXiv:1304.0670 [gr-qc]].
- [7] P. W. Graham and S. Jung, arXiv:1710.03269 [gr-qc].
- [8] S. Hawking, Mon. Not. Roy. Astron. Soc. **152**, 75 (1971).
- [9] B. J. Carr and S. W. Hawking, Mon. Not. Roy. Astron. Soc. **168** (1974) 399.
- [10] E. W. Kolb and I. I. Tkachev, Phys. Rev. Lett. **71**, 3051 (1993) doi:10.1103/PhysRevLett.71.3051 [hep-ph/9303313].
- [11] E. W. Kolb and I. I. Tkachev, Astrophys. J. **460**, L25 (1996) doi:10.1086/309962 [astro-ph/9510043].
- [12] T. Bringmann, C. Kiefer and D. Polarski, Phys. Rev. D **65** (2002) 024008 doi:10.1103/PhysRevD.65.024008 [astro-ph/0109404].
- [13] D. Blais, T. Bringmann, C. Kiefer and D. Polarski, Phys. Rev. D **67**, 024024 (2003) doi:10.1103/PhysRevD.67.024024 [astro-ph/0206262].
- [14] V. Berezhinsky, V. Dokuchaev and Y. Eroshenko, Phys. Rev. D **68**, 103003 (2003) doi:10.1103/PhysRevD.68.103003 [astro-ph/0301551].
- [15] J. Diemand, B. Moore and J. Stadel, Nature **433**, 389 (2005) doi:10.1038/nature03270 [astro-ph/0501589].
- [16] K. M. Zurek, C. J. Hogan and T. R. Quinn, Phys. Rev. D **75**, 043511 (2007) doi:10.1103/PhysRevD.75.043511 [astro-ph/0607341].

- [17] M. Ricotti and A. Gould, *Astrophys. J.* **707**, 979 (2009) doi:10.1088/0004-637X/707/2/979 [arXiv:0908.0735 [astro-ph.CO]].
- [18] M. Kopp, S. Hofmann and J. Weller, *Phys. Rev. D* **83**, 124025 (2011) doi:10.1103/PhysRevD.83.124025 [arXiv:1012.4369 [astro-ph.CO]].
- [19] E. Hardy, *JHEP* **1702**, 046 (2017) doi:10.1007/JHEP02(2017)046 [arXiv:1609.00208 [hep-ph]].
- [20] P. Tisserand *et al.* [EROS-2 Collaboration], *Astron. Astrophys.* **469**, 387 (2007) doi:10.1051/0004-6361:20066017 [astro-ph/0607207].
- [21] S. Calchi Novati, S. Mirzoyan, P. Jetzer and G. Scarpetta, *Mon. Not. Roy. Astron. Soc.* **435**, 1582 (2013) doi:10.1093/mnras/stt1402 [arXiv:1308.4281 [astro-ph.GA]].
- [22] R. J. Nemiroff, V. G. Bistolos, *Astrophys. J.* **358**, 5 (1990) doi:10.1086/168957
- [23] P. N. Wilkinson *et al.*, *Phys. Rev. Lett.* **86**, 584 (2001) doi:10.1103/PhysRevLett.86.584 [astro-ph/0101328].
- [24] B. Carr, F. Kuhnel and M. Sandstad, *Phys. Rev. D* **94**, no. 8, 083504 (2016) doi:10.1103/PhysRevD.94.083504 [arXiv:1607.06077 [astro-ph.CO]].
- [25] T. T. Nakamura, *Phys. Rev. Lett.* **80**, 1138 (1998). doi:10.1103/PhysRevLett.80.1138
- [26] R. Takahashi, *Astrophys. J.* **835**, no. 1, 103 (2017) doi:10.3847/1538-4357/835/1/103 [arXiv:1606.00458 [astro-ph.CO]].
- [27] P. Schneider, J. Ehlers, E. E. Falco, “Gravitational Lenses,” Springer
- [28] R. Takahashi and T. Nakamura, *Astrophys. J.* **595**, 1039 (2003) doi:10.1086/377430 [astro-ph/0305055].
- [29] B. P. Abbott *et al.* [LIGO Scientific and Virgo Collaborations], *Phys. Rev. Lett.* **116**, no. 13, 131103 (2016) doi:10.1103/PhysRevLett.116.131103 [arXiv:1602.03838 [gr-qc]].
- [30] C. Cutler and E. E. Flanagan, *Phys. Rev. D* **49**, 2658 (1994) doi:10.1103/PhysRevD.49.2658 [gr-qc/9402014].
- [31] M. Dominik *et al.*, *Astrophys. J.* **806**, no. 2, 263 (2015) doi:10.1088/0004-637X/806/2/263 [arXiv:1405.7016 [astro-ph.HE]].
- [32] K. Belczynski, D. E. Holz, T. Bulik and R. O’Shaughnessy, *Nature* **534**, 512 (2016) doi:10.1038/nature18322 [arXiv:1602.04531 [astro-ph.HE]].
- [33] J. B. Muoz, E. D. Kovetz, L. Dai and M. Kamionkowski, *Phys. Rev. Lett.* **117**, no. 9, 091301 (2016) doi:10.1103/PhysRevLett.117.091301 [arXiv:1605.00008 [astro-ph.CO]].
- [34] A. Gould, *Astrophys. J.* **386**, L5 (1992) doi:10.1086/186279
- [35] A. Barnacka, J. F. Glicenstein and R. Moderski, *Phys. Rev. D* **86**, 043001 (2012) doi:10.1103/PhysRevD.86.043001 [arXiv:1204.2056 [astro-ph.CO]].

Appendix A: SNR Distribution Function

The observed SNR depends on various parameters of source and detector. The binary masses and the distance are foremost important source parameters. Even for fixed mass and distance, observed SNR varies with: sky location with respect to the detector orientation, GW polarization, binary-orbit inclination as well as spin effects albeit small. The optimal (or, maximum) SNR ρ_{\max} is measured if the binary is facing head-on from top of the detector plane. With uniform distributions of other source parameters, the observed SNR $\rho = \rho_{\max} w$ is distributed according to a cumulative probability distribution $P(w)$ used in Eq. (11). The distribution was obtained by Monte Carlo simulation and was parameterized as [31]

$$P(w) = a_2^{(n)} x^2 + a_4^{(n)} x^4 + a_8^{(n)} x^8 + \left(1 - a_2^{(n)} - a_4^{(n)} - a_8^{(n)}\right) x^{10} \quad (16)$$

where $x \equiv 1 - w/\alpha^{(n)}$ and coefficients a and α are given in the reference. The cumulative distribution is defined to have $P(0) = 1$ and $P(w_{\max}) = 0$, where $w_{\max} = 1$ or 1.4 for 1 or 3 aLIGO detectors.

The optimal sensitivity of a single aLIGO detector, ρ_{\max} , for the redshifted $M_1 = M_2 = 30M_{\odot}$ is estimated in Ref. [29] (our own estimation is also within 20% of this result). Normalized to this $30M_{\odot}$ result, we calculate the optimal sensitivity for all other binary masses.

Appendix B: Strongly Time-Delayed GW Images from Heavy DM

Can LIGO detect the GW fringe induced by arbitrarily heavy lens $M_{\text{DM}} \gtrsim 10^5 M_{\odot}$ (where we stop showing fringe search results in Fig. 5)? In principle, fringe exists. But there are practical limitations for detecting them:

(1) If $f\Delta t_d \gg 1$, then the modulation becomes too quick to be temporally resolved (and frequency-dependent amplification is absent due to the geometric optics). The heavier the lens, the larger time-delay and $f\Delta t_d$. We can roughly require the uncertainty $\delta f \sim 1/N_{\text{cyc}} \sim 1/\mathcal{O}(100 - 1000) \lesssim 1/\Delta t_d$, which means $\Delta t_d \lesssim 100 - 1000$ sec. But it is beyond the scope of this paper to discuss this issue better.

(2) Δt_d also has to be much smaller than the whole duration during which the first wave persists in the LIGO band. Otherwise, we will observe two GWs arriving at well-separated time, instead of fringe. For example, the time taken to reach $f = 20$ Hz since the GW has entered the LIGO band $f = 10$ Hz is 2.5 (80) seconds for $\mathcal{M}_z = 40(5) M_{\odot}$. If we strictly require Δt_d less than these times to produce fringe, we end up with $y \lesssim 5$ and $M_{\text{DM}} \lesssim 10^4 M_{\odot}$ for binary masses $\mathcal{M}_z \lesssim 40 M_{\odot}$. Based on these estimates, we conservatively stop showing fringe search results for $M_{\text{DM}} \gtrsim 10^5 M_{\odot}$ in Fig. 5.

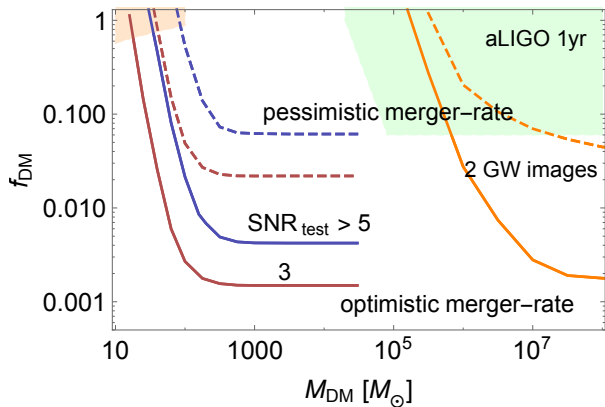


FIG. 6. Same as in Fig. 5, but constraints from strongly time-delayed GW searches are shown together.

In the rest of this Appendix, we approximately calculate the detection rate of strongly time-delayed GW images for heavy DM $M_{\text{DM}} \gtrsim 10^5 M_{\odot}$. The signal is two time-delayed GWs coming from the same direction with different amplitudes; they should have the same observed dimensionless source parameters. We naively require $\Delta t_d \geq 600$ sec and both $\text{SNR} \geq 8$. Assuming no such signal will be observed at three aLIGO detectors, we show the resulting constraints on f_{DM} in Fig. 6.

The time-delayed signal does probe heavy DM region well with similar sensitivity to that of fringe. Importantly, the result makes it clear that GW fringe extends GW lensing probe to significantly lighter and smaller structures.

Appendix C: Supplementary Results

We show some detailed distributions of lensing-detected sources in Fig. 7. Most detections are made from $y \lesssim 2$, yet $y \gtrsim 2$ particularly from heavy binaries do contribute significantly. It is because heavy binaries do merge early at low frequencies so that frequency-dependent modulation with large $f\Delta t_d$ can lead to more pronounced fringe pattern than frequency-dependent amplification that is hardly distinguished from constant amplification due to the short range of frequency. As discussed in main text, large- y can still lead to $\mathcal{O}(1)\%$ amplification/modification of GW amplitudes, resulting in $\epsilon \sim 5 - 25\%$ (not so small).

Another to see from Fig. 7 is that most detections are from sources at $z_S \leq 2$. It is consistent with the detection horizon of a single aLIGO detector: $z_S \sim 1.5$ [29]. This is already comparable to or farther than supernova-Ia detection horizon $z \sim 2$. Having more LIGO-band detectors with improved sensitivities in the near future will surely lead to many GW lensing fringe detections from $z_S \sim 2 - 4$.

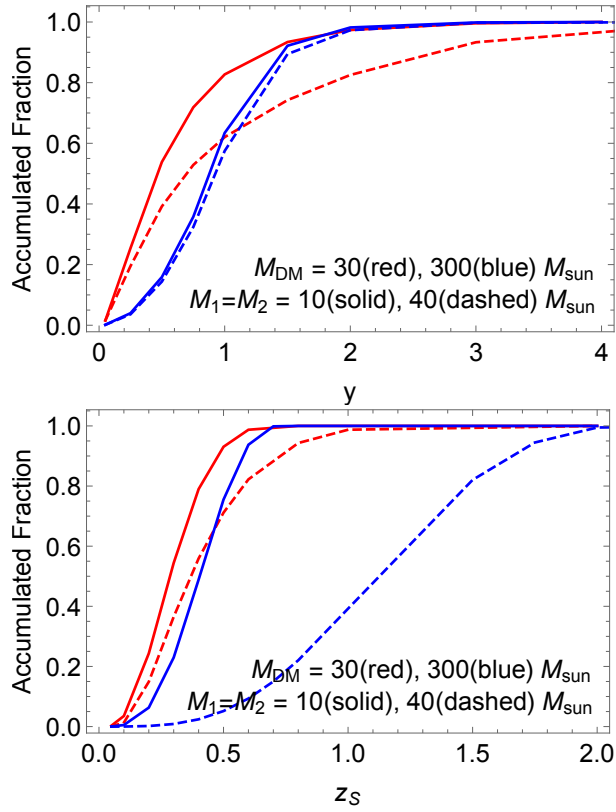


FIG. 7. Accumulated fraction of lensing detection with y (upper) and z_s (lower). The lensing DM masses are $M_{\text{DM}} = 30$ (red) and $300 M_{\odot}$ (blue), and the redshifted GW binary masses are $M_1 = M_2 = 10$ (solid) and 40 (dashed) M_{\odot} . $\text{SNR}_{\text{test}} > 3$ is used.